Journal of
MATERIALS RESEARCH

Microstructure of cosputter-deposited metal- and oxide-MoS_2 solid lubricant thin films

M. R. Hilton[a)]
Mechanics and Materials Technology Center, The Aerospace Corporation, El Segundo, California 90245

G. Jayaram and L. D. Marks
Department of Materials Science and Engineering, Northwestern University, Evanston, Illinois 60208

(Received 10 March 1997; accepted 15 July 1997)

The effect of cosputtering small amounts of Ni (3%, 9%) and SbO_x (20%) on the final microstructure of MoS_2 lubricant thin films has been studied using a combination of scanning and transmission electron microscopy imaging, and electron and x-ray diffraction techniques. The early-growth, near-interface microstructure of both MoS_2 and 3% Ni–MoS_2 cosputtered films is revealed to be a mixture of (002) basal and elongated, large-size (100) and (110) edge islands. Cosputtering with 9% Ni induces a dramatic change in the microstructure, i.e., primarily basal domains with very small isolated regions of edge islands, while cosputtering with 20% SbO_x produces films having no long-range order. The results are compared with and are consistent with previously published x-ray absorption fine structure data. The impact of film morphology on tribological performance is discussed.

I. INTRODUCTION

Sputter-deposited films of MoS_2 have been used as solid lubricants on a variety of spacecraft mechanisms.[1] Most of the early applications included low-cycle devices such as release and deployment mechanisms. The earliest generation of these films had strong (100) and (110) crystal orientation parallel to the substrate, i.e., the low-shear-strength (001) orientation was perpendicular to the substrate, with a columnar plate zone 2 morphology (Thornton model[2]) having significant porosity.[3,4] [The zone models use the dominant diffusion mechanism operating during growth as a classification criterion. Zone 2 films result when surface diffusion dominates; this structure consists of well-defined columnar grains that are generally crystalline. MoS_2 zone 2 have a columnar-plate structure. A zone 1 structure is the result of limited (or absent) adatom mobility that is insufficient to overcome the effect of shadowing favored at low T/T_m (deposition and melting temperatures, respectively) and high gas pressures. The morphology of the zone 1 films consists of large dome-shaped grains that have poorly defined fibrous interiors. These films can be amorphous or crystalline. There is also a zone T (transition) morphology, favored by lower gas pressures and a higher T/T_m that has a structure between the zone 1 and 2 structures. The zone T material has the zone 1 fibrous interior but with flat tops and it is not porous.]

In MoS_2 films, the zone 2 morphology has several disadvantages. Most of the film is in the wrong orientation for lubrication, since the basal planes are perpendicular to the substrate. During sliding contact, these plates detach and reorient into lubricating particles. The porosity of the microstructure promotes detachment near the film-substrate interface, i.e., most of the film becomes loose particles almost immediately. It was recently reported that spallation of MoS_2 films can occur over large areas of contact, generating large debris in addition to the smaller debris of the reoriented columnar grains.[5–7] This spallation was observed to occur early in rolling element bearing tests, which subsequently precipitated significant polymer transfer from the bearing retainers, which in turn caused unacceptable torque noise.[8] Although it is now accepted that MoS_2 films lubricate by intercrystalline slip,[9] the generation of significant film debris early in contact has been considered undesirable, because long endurance becomes dependent upon the retention or recirculation of the film particles in the contact zone, rather than on the gradual wearing away of the film.

Recently, films with new types of microstructures have become available and are being investigated for higher cycle precision applications, such as antenna gimbal bearings. For example, Ni or Au–20% Pd metal multilayers were used to produce dense microstructures having no (100) and (110) edge-plane orientation, and some (002) basal-plane orientation, as determined by x-ray diffraction (XRD).[10] In a recent high-resolution transmission electron microscopy (HREM) study, we reported that the microstructures of Au–20%Pd/MoS_2 multilayer films consist of basal islands of MoS_2 having short-range order.[11] Edge islands are also present, but their growth is interrupted by the presence of the metal layers, even if such layers are not continuous; i.e.,

a)Author to whom correspondence should be addressed.

discrete metal islands at low metal contents (9% to 15%) are observed.

An alternative approach to incorporating multilayers is to use cosputtered dopants, such as Ni, Au, or SbO_x. The hardware necessary for preparing cosputtered films is less complex than apparatus needed for making multilayer films. Cosputtered SbO_x films, in particular, are reported to have good tribological performance in sliding contact.[12–14] (Sb_2O_3 powder has been shown to be an effective tribological additive in burnished and bonded MoS_2 lubricant films.[15])

Recently, two studies reported characterization, via x-ray absorption fine structure (EXAFS) and x-ray photoelectron spectroscopy (XPS), of MoS_2 films incorporating cosputtered Ni or SbO_x, or multilayers of Ni or Au–20%Pd.[16,17] The studies showed that the metal-containing films consist of a $MoS_{2-y}O_y$ phase coexisting with the MoS_2 phase, consistent with earlier findings on pure MoS_2 films.[18] The $MoS_{2-y}O_y$ phase exhibited a MoS_2-like structure, with oxygen substituting for sulfur atoms in the MoS_2 lattice. The amount of the $MoS_{2-y}O_y$ phase could be as high as 25 times that of

TABLE I. List of deposition times (s) of films prepared and estimates of film thickness (nm) based on deposition rates determined from thicker (1- to 5-micron) films.

Deposition run	1		2		3		4	
Film type	Time	Thickness	Time	Thickness	Time	Thickness	Time	Thickness
Pure MoS_2	···	···	16	10.0	16	10.0	50	30.6
	···	···	41	25.0	41	25.0	100	61.2
	···	···	65	40.0	65	40.0	150	91.8
3% Ni	25	11.0	···	···	23	10.0	50	21.7
	55	23.5	···	···	58	24.8	100	43.5
	95	41.0	···	···	93	40.1	150	65.2
9% Ni	35	10.0	139	40.0	35	10.0	50	14.4
	90	26.0	191	55.0	87	25.0	100	28.7
	140	40.0	243	70.0	139	40.0	150	43.0
20% SbO_x	60	11.6	129	25.0	52	10.0	50	9.7
	135	26.0	207	40.0	130	25.0	100	19.3
	225	43.5	284	55.0	207	40.0	150	29.0

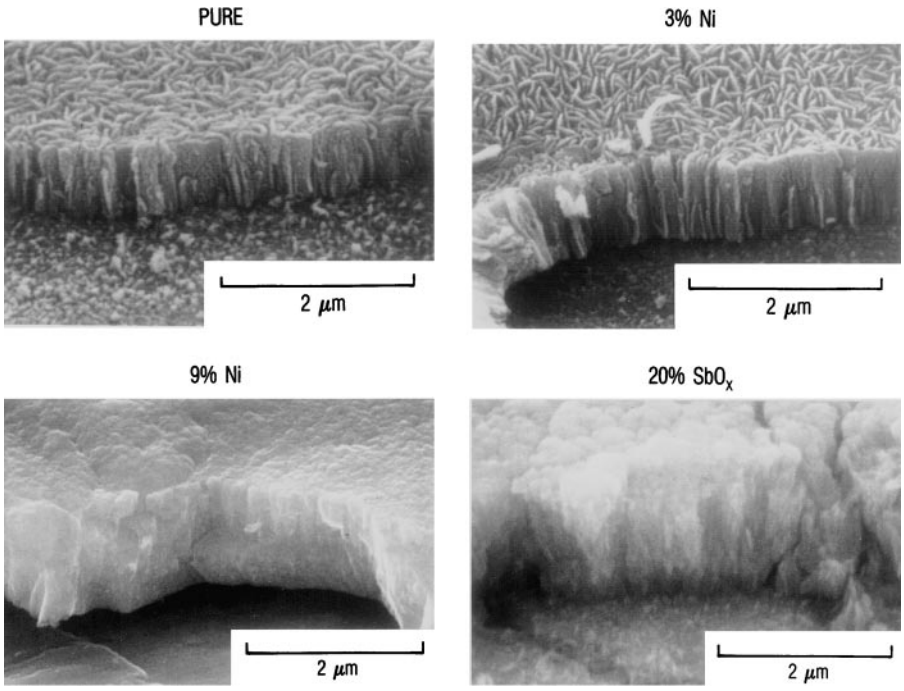

FIG. 1. Cross-sectional SEM micrographs of thicker MoS_2 films prepared on 440C steel substrates. The cross sections were prepared by brale indentation. The pure and 3% films have a columnar-plate zone 2 morphology. Increasing the Ni concentration to 9% yields a fibrous zone T morphology. Cosputtering with 20% SbO_x also yields a dense morphology that has some cauliflower-like features (zone 1 morphology).

the MoS_2 phase. Increasing oxygen content (up to 40% was detected in SbO_x films) correlated with increasing values of y in the $MoS_{2-y}O_y$ phase as well as with decreasing relative amounts of the pure MoS_2 phase. Greater amounts of the $MoS_{2-y}O_y$ phase corresponded to greater disorder in the films. For the Ni-containing films, EXAFS showed that the Ni had not reacted chemically with either $MoS_{2-y}O_y$ or MoS_2, but formed a disordered NiO phase. Short-range order decreased slightly with increasing Ni content. Films cosputtered with SbO_x had little or no short-range order.

These EXAFS studies did not provide data, however, on the effect of the additives on the final microstructure of the metal cosputtered MoS_2 films. In this paper, we report a companion study of the micro- and nanostructures of these films using scanning electron microscopy (SEM) and transmission electron microscopy (TEM), and HREM, in combination with electron and x-ray diffraction (XRD). The data on cosputtered Ni- and SbO_x-MoS_2 films are compared to our available data from EXAFS, to SEM and XRD data on similar films published by Zabinski *et al.*,[14] and to EXAFS and HREM data from other MoS_2 films.

II. EXPERIMENTAL PROCEDURES

MoS_2 films were prepared by direct current (dc) triode sputtering, using equipment reported previously.[19,20] Deposition conditions included: substrate temperature of 190 °C, pressure of 2.9 Pa, and power density of 2 W/cm^2. Cosputtering was accomplished by sputtering from rod targets of compressed MoS_2 powder and of Ni or of $MoS_2-Sb_2O_3$. Four nominal compositions were prepared: Pure, 3% Ni, 9% Ni, and 20%Sb_2O_3. For TEM studies, thin films were prepared on amorphous carbon TEM grids with deposition times as listed in Table I. Nominal thicknesses are also listed that are based on deposition rates of thicker films, e.g., 1 to 5 μm. The time of deposition, however, may be a better gauge of the amount of material present in the near-interface films prepared for TEM, since the film growth rates might differ in the early stages of film deposition. In all, four groups of deposition runs were prepared over three years. Conventional TEM was performed on films from the first three deposition runs using a Phillips EM-420 microscope operated at 120 kV, while HREM was performed on films from the fourth deposition run using a Hitachi H-9000 microscope operating at 300 kV.

Films, 1 to 5 μm in thickness, were also prepared during separate deposition runs, on 440C steel flats (polished using 0.3 μm alumina grit). The morphologies of these thicker films were characterized in cross section by SEM after indentation fracture,[21] and the crystalline orientations of these films were assessed using XRD.[4]

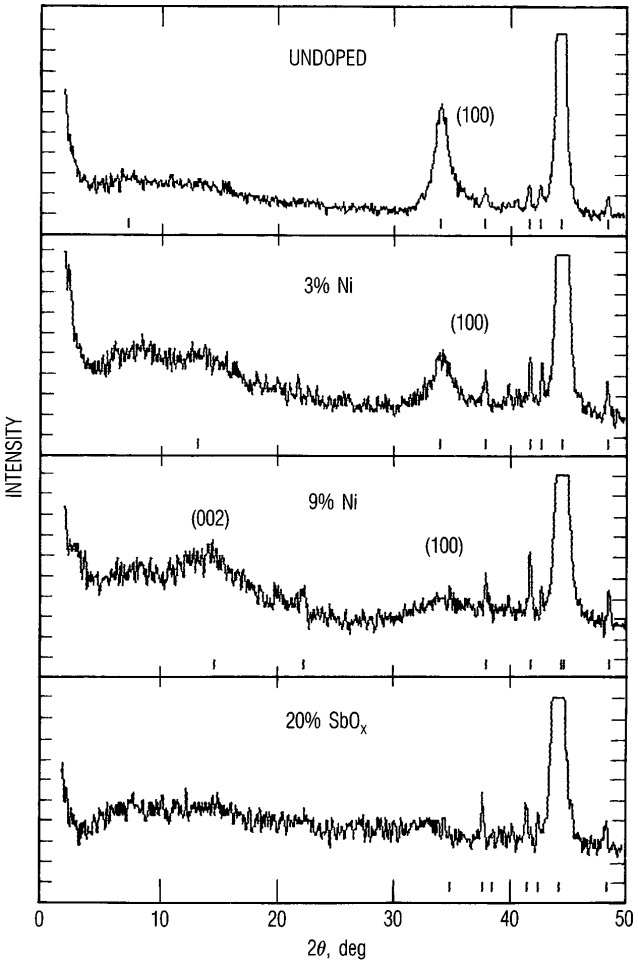

FIG. 2. XRD diffractograms of the films shown in Fig. 1. The bulk of the pure and 3% Ni films have edge-plane preferred orientation. [The weak x-ray signal originating from the thin, near-interface structure of the films that consists of (002) basal planes and (100)/(110) edge planes is not effectively detected by XRD.] The presence of 9% Ni results in a poorly crystalline material with both basal and edge plane contributions. The mixed orientation suggests that competitive growth, i.e., domination of one orientation at the expense of others, is suppressed. The films containing 20% SbO_x are disordered with respect to XRD—no MoS_2 peaks are observed. Adatom mobility during growth appears to have been limited. (Unlabeled peaks represent the 440C steel substrate.)

III. RESULTS

A. Scanning electron microscopy

SEM reveals that the pure and 3% Ni films have a columnar-plate zone 2 morphology (Thornton model[2]) consistent with other undoped sputter-deposited films grown at this or similar pressures, as shown in Fig. 1.[3,4,14,22,23] Highly doped Ni or SbO_x cosputtered films are dense but have a fibrous morphology that might be classified as zone T or possibly zone 1. In contrast, multilayer films are also dense (i.e., do not have obvious pores), but show no apparent structure.[10]

Both the zone 1 and zone T morphologies are indicative of limited adatom mobility during deposition.

B. X-ray diffraction

XRD shows that the crystallites in pure and 3% Ni films have their (100) and (110) planes preferentially oriented parallel to the substrate; the (100) portions of the diffractograms are shown in Fig. 2. Diffractograms of 9% Ni–MoS_2 films reveal a predominant (002) orientation with a relatively smaller portion having the (100) and (110) planes parallel to the substrate. The mixed orientation suggests that rapid growth of edge islands is suppressed. No long-range order was detected in the SbO_x films by XRD.

C. Transmission electron microscopy

1. Conventional TEM

Conventional TEM at 120 kV allows mainly the (002) type lattice fringes to be observed. Plan-view lattice images of nominal 40-nm-thick films of the four compositions are shown in Fig. 3. These films were prepared in Runs 1 and 2. For pure and 3% Ni films, a mixture of basal and edge islands is observed via lattice imaging and dark field imaging (not shown), similar to results obtained in an earlier TEM study of rf sputter-deposited films that were not metal-doped.[23] The edge islands are anisotropic, in that the width along the basal plane ⟨001⟩ direction is less than the length along the edge plane ⟨100⟩ or ⟨110⟩ directions. The edge islands appear to be growing above, and shadowing the adjacent basal islands; the edge island density increases with deposition time for films of a particular composition. For 9% Ni films, the nanostructure consists of edge islands that are more isotropic in the basal ⟨001⟩ and edge ⟨100⟩/⟨110⟩ directions, as shown in Fig. 4. The edge islands in this case do not appear to shadow the basal islands; i.e., the basal island growth seems to be competitive with edge island growth. The SbO_x films appear featureless in these TEM micrographs.

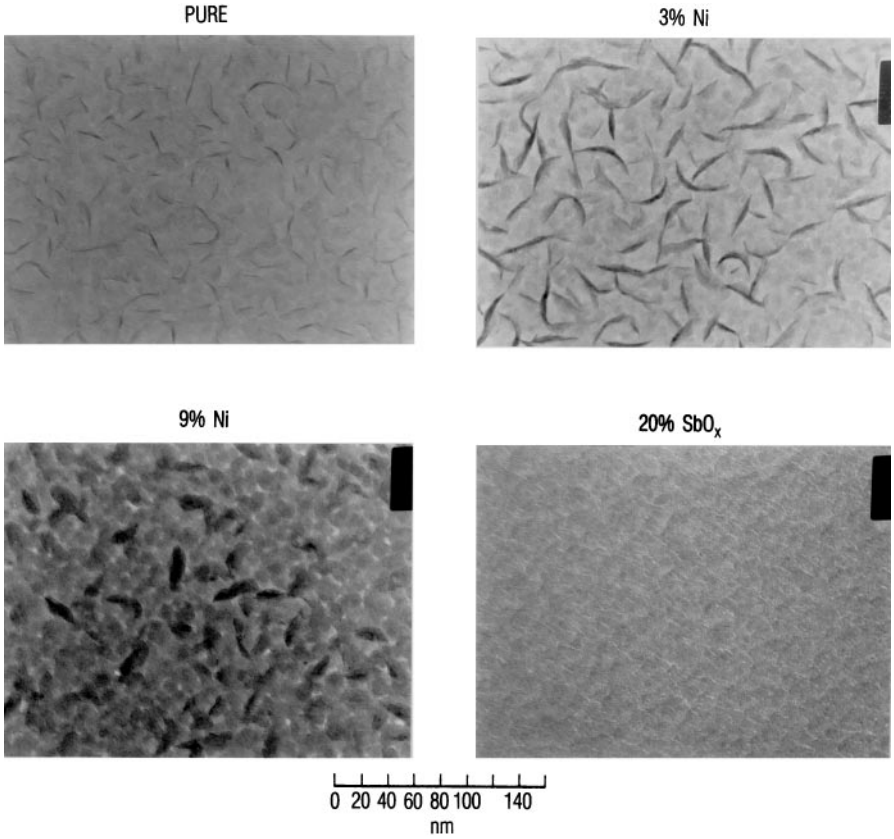

FIG. 3. Conventional TEM (002) lattice images of the early-growth nanostructure of Run 1-2 MoS_2 films deposited on carbon as a function of Ni or SbO_x content. The pure and Ni films have mixtures of edge and basal islands. However, the 9% Ni films have shorter but thicker edge islands (see Fig. 4). The 20% SbO_x films have a nanostructure that contains isotropic equiaxed features. This morphology is consistent with films having limited adatom mobility and poor crystallinity. The films were selected from Runs 1 and 2 and had nominal thicknesses of 40 nm, based on growth rates determined from thicker films. As noted in the text, these film growth rates may not be valid during the early phases of growth due to competitive nucleation and growth that occurs, yielding less porous morphologies near the film-substrate interface than those found in some of the thicker films of different composition. The deposition times (s) for the films are as follows: pure (65), 3% Ni (95), 9% Ni (140), and 20% SbO_x (207).

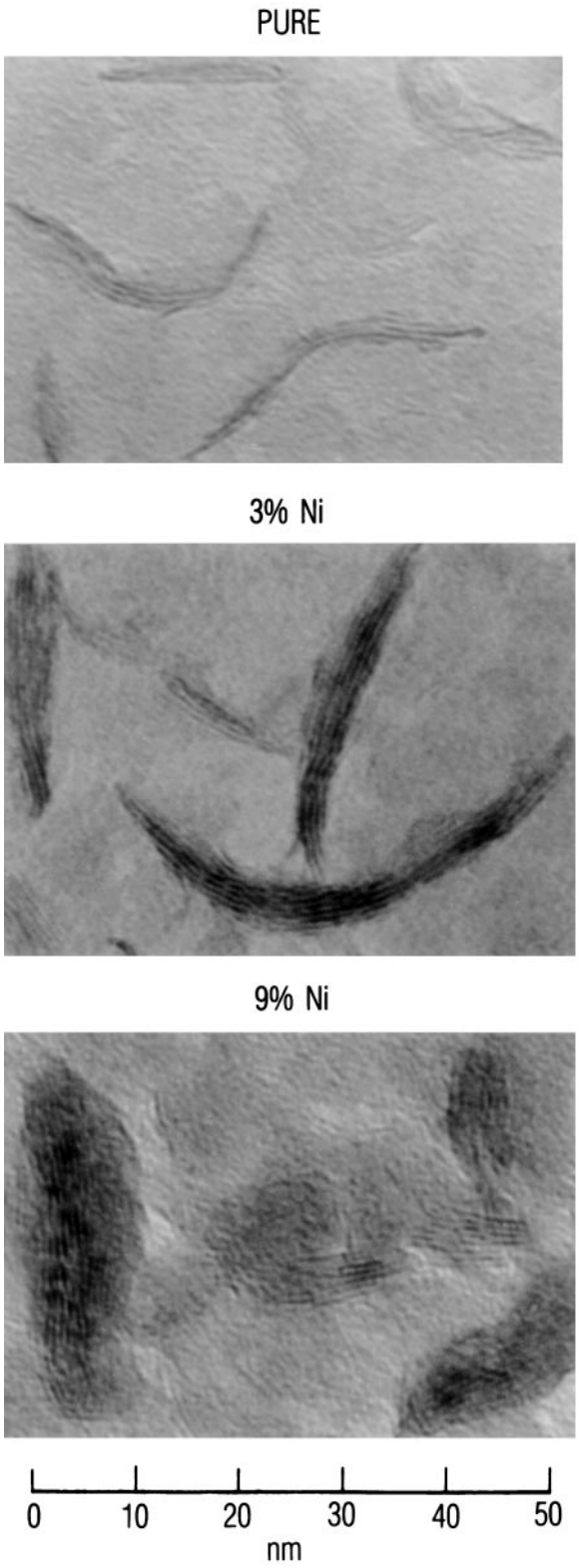

FIG. 4. Conventional TEM (002) lattice images of the pure, 3% Ni, and 9% Ni films taken at higher magnification than the micrographs in Fig. 3. The 9% Ni films have edge islands of less length, but greater width. The nominal film thicknesses would be 40 nm based on growth rates determined from thicker films. The deposition times (s) for the films are as follows: pure (65), 3% Ni (95), and 9% Ni (140).

An assessment of the morphological data and energy dispersive spectroscopy (EDS) data also obtained in the TEM of the first three deposition runs indicated that the estimated film thicknesses for different compositions may be inaccurate, since these thickness values are extrapolated from interferometric measurements of thicker films.[24] These estimates do not account for differences in porosity that develop in thicker films of different composition. Deposition rates calculated from these thick-film measurements do decrease with increasing Ni or SbO_x content. It is expected that the rate of film deposition, measured in mass per unit time, can and does change with target composition at fixed power. However, due to the dramatic transition from basal to edge orientation above the substrate in the pure and 3% Ni films, the estimated thicknesses of these TEM film specimens are probably overestimates. This ambiguity led to a comparison of films having identical deposition times, i.e., deposition Run 4.

2. High resolution electron microscopy

HREM images of the Run 4 MoS_2 and Ni–MoS_2 films show the coexistence of basal and edge islands, for all compositions analyzed. The 20% SbO_x–MoS_2 films also have some edge islands, but their occurrence is a few orders of magnitude less than the other films. For a deposition time of 150 s, nearly identical microstructures were seen in the case of both pure and 3% Ni cosputtered MoS_2 films. The morphology in the two cases was dominated primarily by edge islands, with regions of short-range-ordered basal islands, which can be imaged by HREM. The short-range order of the basal islands appears to decrease with higher Ni or SbO_x content, as will be discussed in the next section on diffraction results. The microstructural differences are evident in both Figs. 5 and 6, which are montages of data collected from the films at low and high magnification, respectively. Figure 5 clearly reveals that the population of edge islands decreases dramatically on sputtering with either 20% SbO_x or 9% Ni. Figure 6 shows that edge islands, nearly 10 nm wide and about 40 to 60 nm in length, are seen in both the pure and 3% Ni films; i.e., no changes in the microstructure on adding Ni in this concentration are apparent from the HREM data. If one assumes that the film deposition rate is similar for the pure and 3% Ni films in the very early stages of growth, then there appears to be little difference in nanostructure between these films. Cross-sectional TEM would be required to definitely measure these early-growth film thicknesses accurately. In films cosputtered with 9% Ni, edge islands ranged in width from 2.5 to 4 nm and in length from 5 to 7 nm.

In comparison to films deposited for 150 s, those deposited for 50 s show a decrease in both the fraction and

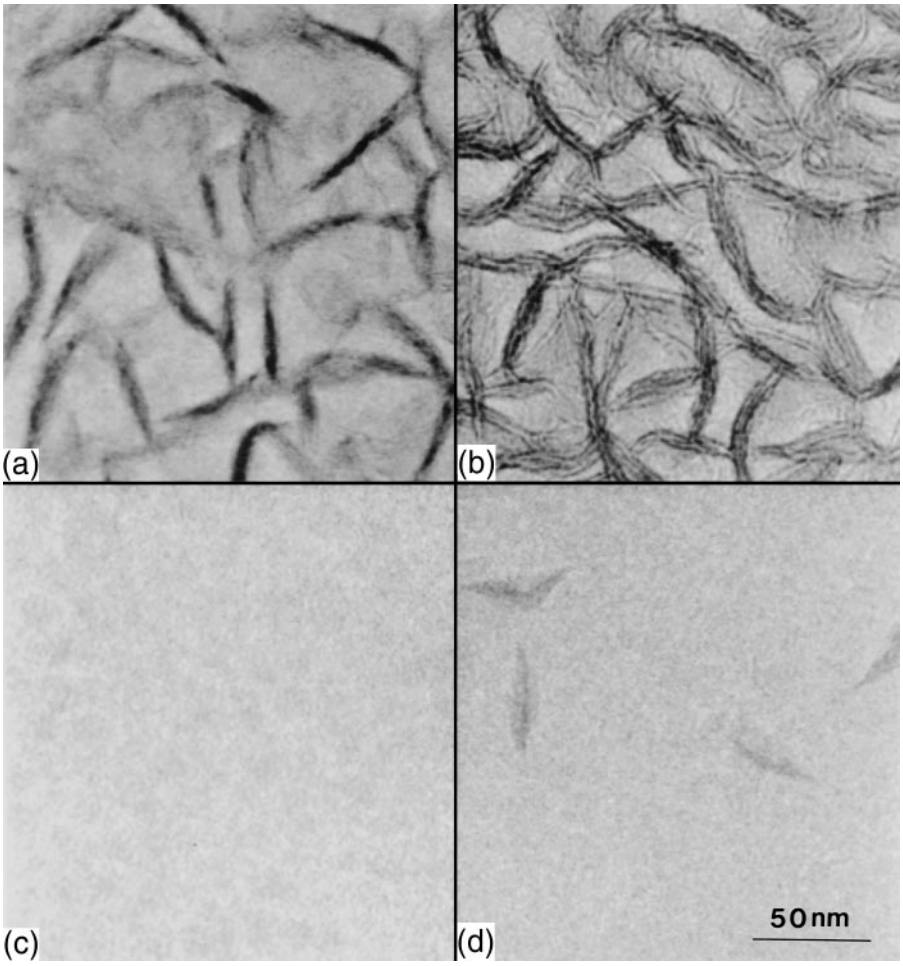

FIG. 5. Montage of HREM images, recorded at low magnification, from Run 4 films of four different compositions, deposited for 150 s: (a) Pure MoS_2, (b) 3% Ni–MoS_2, (c) 9% Ni–MoS_2, and (d) 20% SbO_x–MoS_2. Note the decrease in edge island density in (c) and (d), in comparison to (a) and (b). For identical deposition times, the edge island densities of (a) and (b) are comparable.

size of edge islands; however, the latter still dominate the morphology of pure and 3% Ni films. Edge islands are nearly nonexistent in films cosputtered with either 9% Ni or SbO_x, as seen in Figs. 7 and 8, which show montages of the microstructures of the films observed at low and high magnification, respectively.

3. Transmission electron diffraction

Changes in the microstructure as a function of change in composition (i.e., addition of Ni or SbO_x as a cosputtering agent) are also apparent from selected transmission electron diffraction (TED) data. Figure 9 is a montage of the TED's obtained from the corresponding images in Figs. 5 and 6 (i.e., for deposition time of 150 s); the intensities in the patterns have all been scaled to the same dynamic range to facilitate both qualitative and quantitative comparisons.

The MoS_2 films and Ni cosputtered films are highly polycrystalline in nature. In the case of the pure films, the (100) and (110) rings of the basal islands are clearly seen to coexist with an extremely strong (002) ring, arising from the dominant edge island morphology. A weak (103) ring, due to regions of near-basal orientation, is also seen in these patterns (the feature is poorly transferred in the print reproduction process but was visible in the negatives). Films cosputtered with 3% Ni show a slight decrease in the intensity of the (002) ring, and a sharpening and increase in intensity of the (103) ring, relative to the pure case. Thus, subtle changes in the morphology, in the form of a decrease in the population of edge islands and an increase in that of the near-basal islands, accompany the sputtering process. The dramatic changes in the microstructure seen in HREM images of the 9% Ni cosputtered films are corroborated by corresponding TED data, which show a complete disappearance of both the (002) and (103) rings, in comparison with the pure and 3% Ni films; this is also accompanied by a significant increase in the sharpness and intensity of the (100) and (110) rings. TED patterns from films cosputtered with SbO_x show extremely diffuse, weak rings, suggesting that the grains

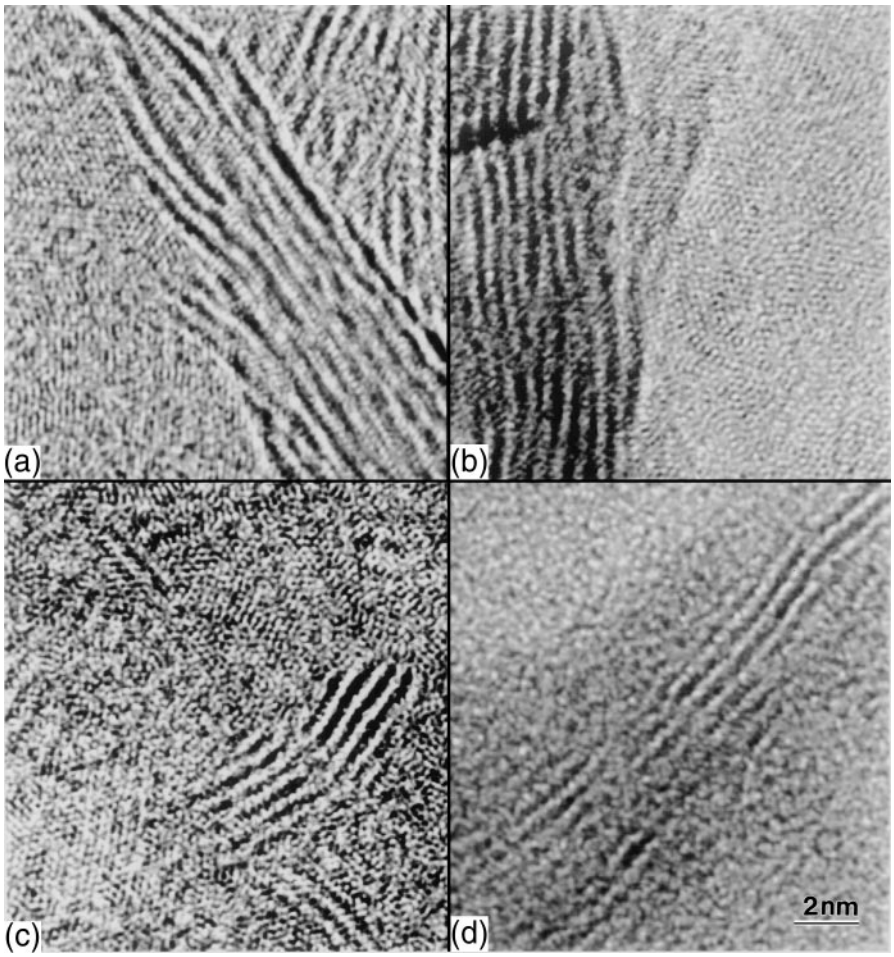

FIG. 6. Montage of HREM images, recorded at higher magnification, from regions in films shown in Fig. 5. Hexagonal basal island domains coexist with edge islands in (a)–(c), while the extreme short range order of basal islands is apparent in (d).

have very short range order. TED patterns (not shown) recorded from these films deposited for 50 s agree well with the corresponding HREM data.

IV. DISCUSSION

The current HREM/TED data on thin films are consistent with earlier EXAFS and XPS data collected from thicker films.[16,17] Incorporation of Ni or SbO_x above a critical amount results in the relative suppression of edge island growth. For films containing 9% Ni, a predominance of basal islands is observed. The HREM/TED data agree with the hypothesis from EXAFS data that the majority of Ni is dispersed in small disordered clusters of NiO, since discrete regions of Ni or NiO were not detected. The presence of NiO appears to interrupt or suppress the rapid growth of edge islands, which allows the basal islands to grow.

For films containing 20% SbO_x, no crystalline order was detected by TED. HREM detected only fragments of edge islands in the 50-s films; the density of these islands increased in the 150 s case but was still very low. The HREM and TED data are consistent with EXAFS, in that little order was detected in the basal island regions of the SbO_x–MoS_2 films. There is one aspect of the EXAFS data that the HREM/TED data cannot confirm—the existence of the $MoS_{2-y}O_y$ phase. HREM and TED do not have sufficient resolution to distinguish between the MoS_2 and $MoS_{2-y}O_y$ phases, which are isostructural. Furthermore, discernment is strongly complicated by the possibility that the two phases could be physically overlapping in various regions, and the HREM/TED data represent superimposed information through the film regions. Note that the EXAFS data reported in Ref. 17 indicate that the SbO_x–MoS_2 films have a large concentration of the $MoS_{2-y}O_y$ phase relative to the MoS_2 phase, e.g., a ratio 10 to 25 : 1. The general disorder in the SbO_x–MoS_2 films may be due, in part, to the large presence of $MoS_{2-y}O_y$ clusters, whose formation is promoted by oxygen transfer from SbO_x.

The presence of the (103) TED rings in pure and 3% Ni films is consistent with the detection of (103)

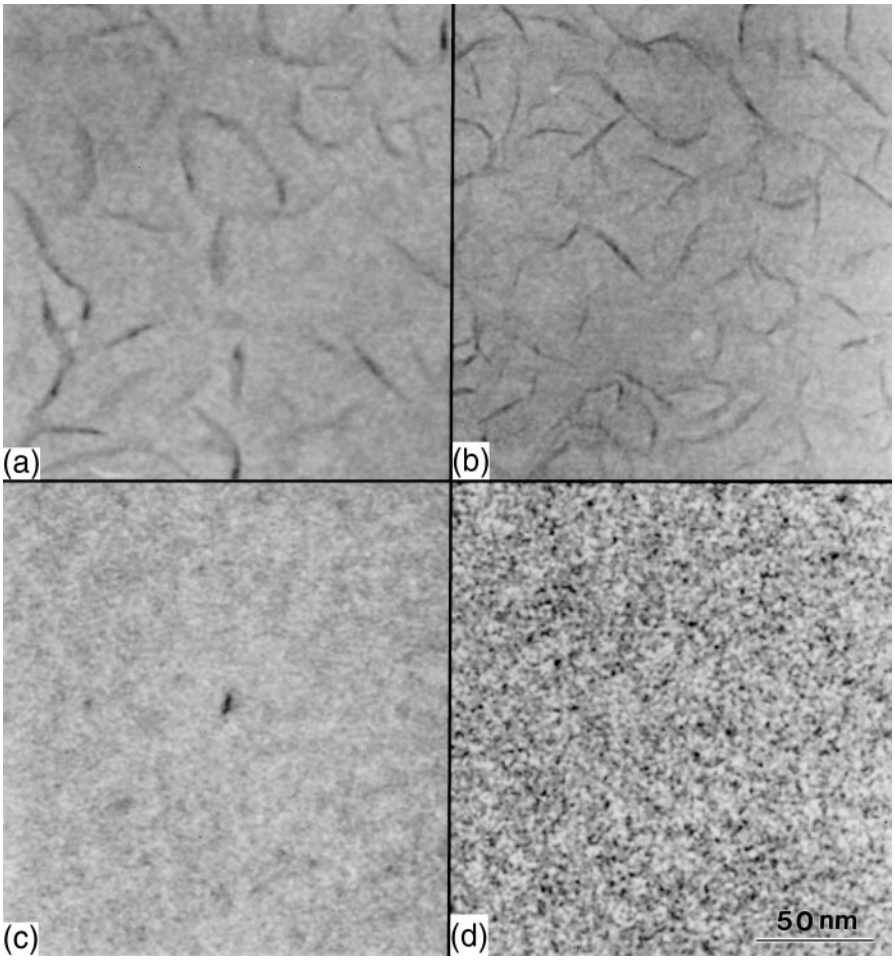

FIG. 7. Montage of HREM images, recorded at low magnification, from films deposited for a total time of 50 s. (a)–(d) represent the same compositions as in Figs. 5 and 6. Note the generic decrease in edge island density, in comparison to Fig. 5.

XRD rings by the Read thin film camera method in other (thicker) pure MoS_2 films grown by rf-diode sputtering.[25] The presence of the (103) reflection suggests that crystalline registry is conserved between the basal plane layers; that is, the stacking of atomic layers is not random. Such random stacking has been reported for some MoS_2 films deposited by rf magnetron methods.[26]

Our SEM observations and XRD data of Ni- and SbO_x–MoS_2 codeposited films are generally consistent with recent results reported by Zabinski *et al.* of films produced by the same manufacturer over a similar time period.[14] They also found increasing densification of morphology and decreasing crystalline order with increasing dopant content. However, there are subtle differences in the XRD results reported here and in their study. We were unable to detect any discernable MoS_2 peaks in our SbO_x codeposited films. They reported barely discernable, broadened (002) peaks and (100) peaks in films containing 35% SbO_x. The difference in results suggests that the degree of crystalline order of the SbO_x–MoS_2 films varies somewhat from deposition run to run, and that the magnitude of this variation can span across the crystalline domain size detection limit of XRD and TED. The relative deposition rate of either Ni or SbO_x relative to MoS_2 may vary somewhat between runs. Comparison of the 9% Ni films from Runs 1–2 and 4 [in Figs. 4(c) and 5(c), respectively] also shows some variation in edge island content for films nominally prepared with the same thickness—the Run 1–2 films have more edge islands than the Run 4 films. The differences may stem from subtle variations in metal deposition rate. It is also possible that the background water vapor pressure may have been (slightly) different between specific deposition runs. Buck has shown that the presence of water vapor during deposition can reduce MoS_2 film crystallinity.[27]

The lack of crystalline order in as-deposited SbO_x films does not appear to be detrimental to tribological performance. Sliding wear tests have shown that the SbO_x–MoS_2 films have better endurance than the Ni–MoS_2 films.[14] Rolling element bearing tests in the Aerospace Corp. laboratory have also shown that

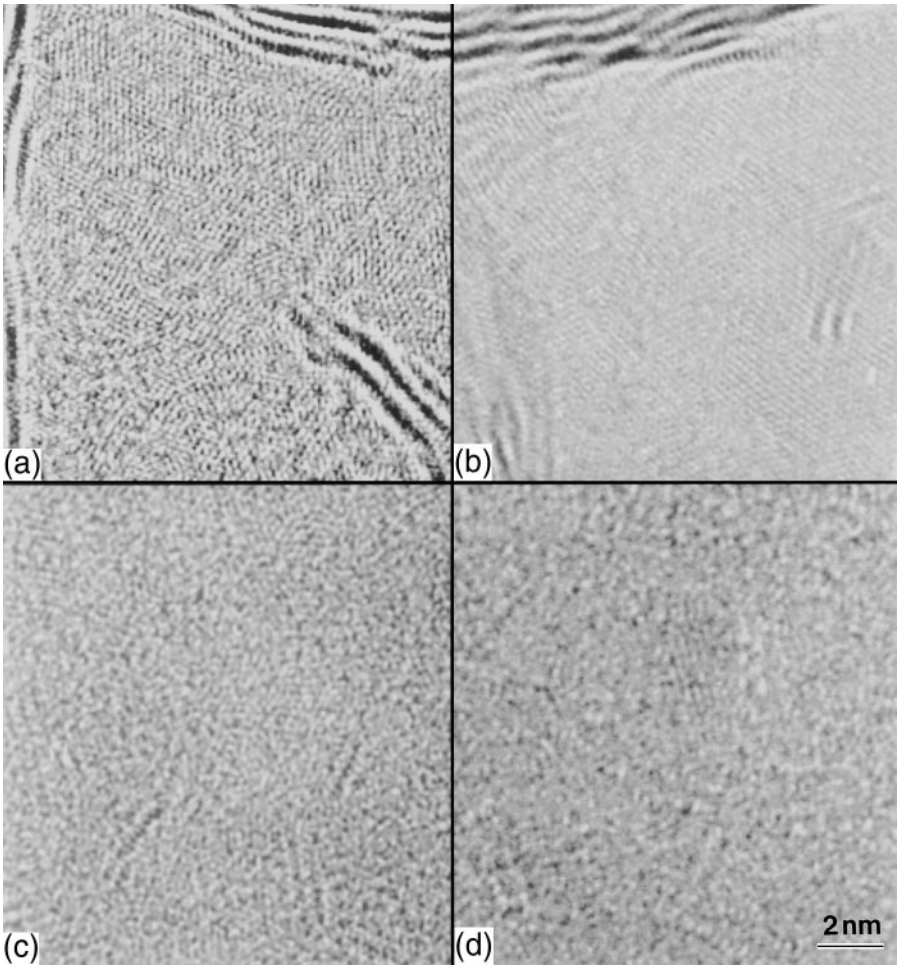

FIG. 8. Montage of HREM images, recorded at higher magnification, from regions in films in Fig. 7. Primarily basal orientation is apparent in (c), in contrast to (a) and (b), while the films in (d) seem to have very short range order, similar to ones in Fig. 6(d).

the SbO_x-MoS_2 films perform better than the $Ni-MoS_2$ films.[7,28] Stress-induced crystallization has been observed after sliding contact in other zone 1 or T morphology films having no detectable long-range order, as determined by XRD, in the as-deposited state.[4] (The zone 1 morphologies in these films were promoted by the presence of water vapor during deposition, which led to formation of cosputtered MoO_3.[29]) It remains to be determined if long-range order develops in the highly doped SbO_x films during sliding or rolling contact.

For applications where lubricant debris is easily ejected, it is desirable that the solid lubricant films wear gradually and do not easily spall. Indentation testing has been reported on both Ni- and SbO_x-MoS_2 cosputtered films and on Ni- and Au/20%Pd$-MoS_2$ multilayer films.[7] The data show that the multilayer films can have higher fracture toughness, depending upon composition. A prior HREM study has shown that the multilayer films can form periodic (i.e., 5 to 10 nm) layers of continuous metal crystallites or discrete metal islands, depending upon metal content.[11] These metal layers and/or islands are believed to improve fracture toughness by creating metal-MoS_2 interfaces that generate additional surface area, and hence absorb additional energy, as spallation radial cracks propagate. In contrast, discrete islands of Ni/NiO or Sb/SbO_x have not been observed in the present study of cosputtered films. For applications in which improved fracture toughness of dense films is desired, multilayer films may be preferred.

V. CONCLUSIONS

A combination of electron microscopy techniques and electron and x-ray diffraction methods has been used to characterize sputter-deposited MoS_2 films containing various amounts of cosputtered Ni or SbO_x. The early-growth, near-interface microstructure of both pure and 3% $Ni-MoS_2$ cosputtered films is revealed to be a mixture of (002) basal and large elongated (100) and (110) edge islands. These films have columnar-plate morphologies with porosity between the plates. Cosputtering with 9% Ni induces a dramatic change in the

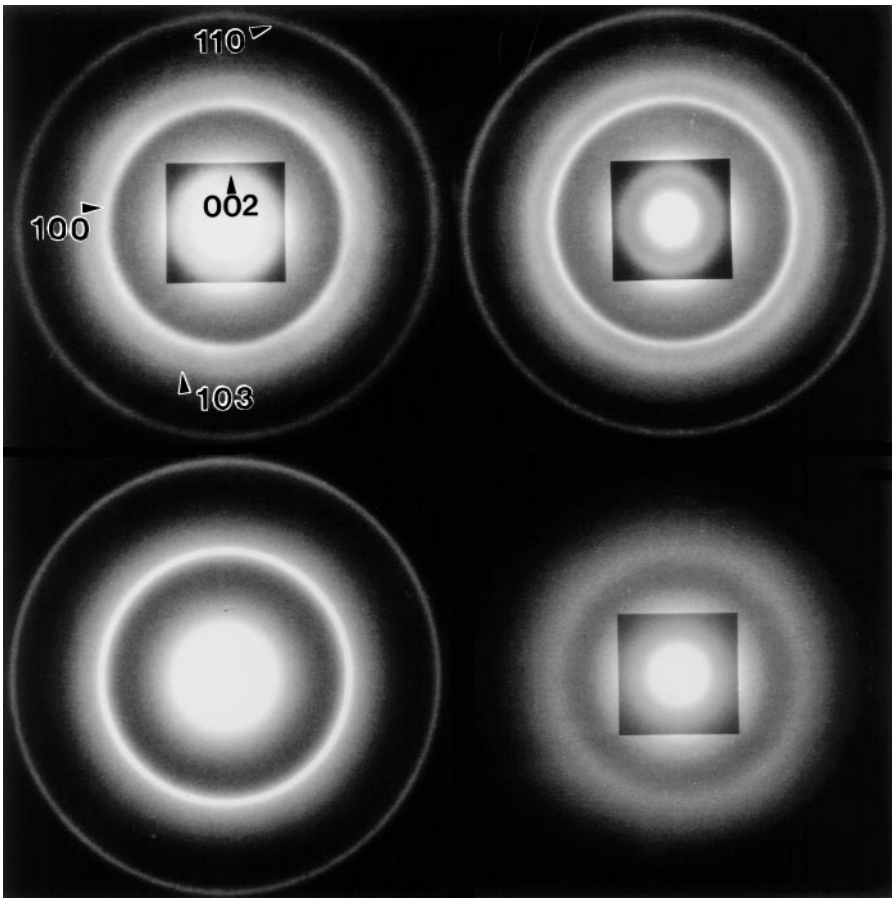

FIG. 9. Montage of TED patterns from corresponding regions in Fig. 6. Insets in all four cases show the region around the transmitted beam, extracted from patterns recorded at a lower exposure time. The (002), (100), (110), and (103) rings are arrowed for reference in the pure film. Note the decrease in intensity of the (002) ring and increase in that of the (100) and (110) rings, with increasing Ni content. Disappearance of the (103) rings between (b) and (c) is indicative of differences in the orientation of the MoS_2 in the near interface region, i.e., a primarily basal-oriented film. Weak and diffuse rings in (d) corroborate the extreme short range order, seen in Fig. 6(d).

microstructure, i.e., primarily basal domains with very small isolated regions of edge islands, while cosputtering with 20% SbO_x produced films having no long-range order. Both the 9% Ni and 20% SbO_x films have dense fibrous morphologies. No discrete islands of Ni/NiO_x or Sb/SbO_x were detected in the films, in contrast to nanostructures found in dense Au–20% Pd metal-multilayer MoS_2 films. The microscopy and diffraction data on these cosputtered films are consistent with previously reported EXAFS data.

ACKNOWLEDGMENTS

This work was supported by the U.S. Air Force Materiel Command, Space and Missiles Systems Center, under Contract FO4701-93-C-0094 as part of The Aerospace Corporation Mission-Oriented Investigation and Experimentation Program and the U.S. Air Force Office of Scientific Research on Grant F49620-94-1-0164 AFOSR. The authors would like to thank B. C. Stupp, R. Gordman, and T. Schneider (Hohman Plating and Manufacturing, Inc.) for preparing cosputtered Ni- and SbO_x–MoS_2 films and Paul Adams (Aerospace) for obtaining the XRD data.

REFERENCES

1. M. R. Hilton and P. D. Fleischauer, Surf. Coat. Technol. **54–55**, 435 (1992).
2. J. A. Thornton, JVSTA **4** (6), 3059, Nov/Dec 1986, and earlier references cited therein.
3. T. Spalvins, ASLE Trans. **14**, 267 (1971); **17**, 1 (1973); Thin Solid Films **96**, 17 (1982).
4. M. R. Hilton and P. D. Fleischauer, in *New Materials Approaches to Tribology: Theory and Applications,* edited by L. E. Pope, L. Fehrenbacher, and W. O. Winer (Mater. Res. Soc. Symp. Proc. **140**, Pittsburgh, PA, 1989), p. 227.
5. G. B. Hopple, J. E. Keem, and S. H. Loewenthal, Wear **162–164**, 919 (1993).
6. G. B. Hopple and S. H. Loewenthal, Surf. Coat. Technol. **68/69**, 398 (1994).
7. M. R. Hilton, Surf. Coat. Technol. **68/69**, 407 (1994).
8. S. H. Loewenthal, R. G. Chou, G. B. Hopple, and W. L. Wenger, Tribol. Trans. **37** (3), 505 (1994).

9. P. D. Fleischauer and R. Bauer, Tribol. Trans. **31** (2), 239 (1988).
10. M. R. Hilton, R. Bauer, S. V. Didziulis, M. T. Dugger, J. Keem, and J. Scholhamer, Surf. Coat. Technol. **53**, 13 (1992).
11. G. Jayaram, L. D. Marks, and M. R. Hilton, Surf. Coat. Technol. **76–77**, 393 (1995) .
12. M. N. Gardos and J. J. Bohner, Technical Report AFML-TR-79-4091, Part II, December (1979).
13. M. T. Lavik, R. D. Hubble, and B. D. McConnell, Lubr. Eng. **31**, 20 (1975).
14. J. S. Zabinski, M. S. Donley, S. D. Walck, T. R. Schneider, and N. T. McDevitt, Tribol. Trans. **38** (4), 894 (1995).
15. J. S. Zabinski, M. S. Donley, and N. T. McDevitt, Wear **165**, 103 (1993), and references cited therein.
16. J. R. Lince, M. R. Hilton, and A. S. Bommannavar, J. Mater. Res. **10**, 2091 (1995).
17. J. R. Lince, M. R. Hilton, and A. S. Bommannavar, Thin Solid Films **264**, 120 (1995).
18. J. R. Lince, M. R. Hilton, and A. S. Bommannavar, Surf. Coat. Technol. **43/44**, 640 (1990).
19. B. C. Stupp, Thin Solid Films **84**, 257 (1981).
20. B. C. Stupp, *Proc. Third Int. Conf. on Solid Lubrication,* **ASLE SP-14**, Soc. Tribologists and Lubrication Engineers (1984), p. 217.
21. M. R. Hilton and P. D. Fleischauer, Thin Solid Films **172**, L81 (1989).
22. C. Muller, C. Menoud, M. Maillat, and H. E. Hintermann, Surf. Coat. Technol. **36**, 351 (1988).
23. M. R. Hilton and P. D. Fleischauer, J. Mater. Res. **5**, 406 (1990).
24. T. Schneider, Hohman Plating and Manufacturing, Inc., Dayton, OH, private communication, June 1, 1992.
25. J. R. Lince and P. D. Fleischauer, J. Mater. Res. **2**, 827 (1987).
26. J. Moser and F. Lévy, Thin Solid Films **240**, 56 (1994).
27. V. Buck, Thin Solid Films **139**, 157 (1986); Vacuum **36**, 89 (1986); Thin Solid Films **198**, 157 (1991).
28. S. V. Didziulis, M. R. Hilton, R. Bauer, and P. D. Fleischauer, "Thrust bearing wear life and torque tests of sputter-deposited MoS2 films," TOR-92(2064)-1, The Aerospace Corporation, October, 1992.
29. M. R. Hilton, R. Bauer, and P. D. Fleischauer, Thin Solid Films **188**, 219 (1990).